**Atmospheric
Chemistry
and Physics
Discussions**

ACPD

8, 827–891, 2008

Ground-based FTIR
measurements at Ile
de La Réunion

C. Senten et al.

Title Page

Abstract | Introduction

Conclusions | References

Tables | Figures

◄◄ | ►►

◄ | ►

Back | Close

Full Screen / Esc

Printer-friendly Version

Interactive Discussion

EGU

Technical Note: New ground-based FTIR measurements at Ile de La Réunion: observations, error analysis, and comparisons with independent data

C. Senten[1], M. De Mazière[1], B. Dils[1], C. Hermans[1], M. Kruglanski[1], E. Neefs[1], F. Scolas[1], A. C. Vandaele[1], G. Vanhaelewyn[1], C. Vigouroux[1], M. Carleer[2], P. F. Coheur[2], S. Fally[2], B. Barret[3], J. L. Baray[4], R. Delmas[4], J. Leveau[4], J. M. Metzger[4], E. Mahieu[5], C. Boone[6], K. A. Walker[6,7], P. F. Bernath[6,8], and K. Strong[7]

[1]Belgian Institute for Space Aeronomy (BIRA-IASB), Brussels, Belgium
[2]Service de Chimie Quantique et Photophysique (SCQP), Université Libre de Bruxelles (ULB), Brussels, Belgium
[3]formerly at BIRA-IASB and SCQP/ULB, now at the Institut d'Aérologie, Toulouse, France
[4]Laboratoire de l'Atmosphère et des Cyclones (LACy), Université de La Réunion, France
[5]Institute of Astrophysics and Geophysics, University of Liège, Liège, Belgium

[6] Department of Chemistry, University of Waterloo, Waterloo, Ontario, Canada
[7] Department of Physics, University of Toronto, Toronto, Ontario, Canada
[8] Department of Chemistry, University of York, Heslington, York, UK

Correspondence to: C. Senten (cindy.senten@aeronomie.be)

Ground-based FTIR measurements at Ile de La Réunion

C. Senten et al.

Title Page

Abstract	Introduction
Conclusions	References
Tables	Figures

|◄ | ►|

◄ | ►

| Back | Close |

Full Screen / Esc

Printer-friendly Version

Interactive Discussion
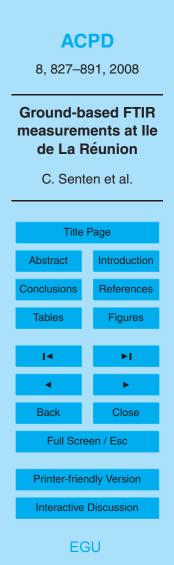
EGU

Abstract

Ground-based high spectral resolution Fourier-transform infrared (FTIR) solar absorption spectroscopy is a powerful remote sensing technique to obtain information on the total column abundances and on the vertical distribution of various constituents in the atmosphere. This work presents results from two short-term FTIR measurement campaigns in 2002 and 2004, held at the (sub)tropical site Ile de La Réunion (21°S, 55°E). These campaigns represent the first FTIR observations carried out at this site. The results include total column amounts from the surface up to 100 km of ozone (O_3), methane (CH_4), nitrous oxide (N_2O), carbon monoxide (CO), ethane (C_2H_6), hydrogen chloride (HCl), hydrogen fluoride (HF) and nitric acid (HNO_3), as well as some vertical profile information for the first four mentioned trace gases. The data are characterised in terms of the vertical information content and associated error budget. In the 2004 time series, the seasonal increase of the CO concentration was observed by the end of October, along with a sudden rise that has been attributed to biomass burning events in southern Africa and Madagascar. This attribution was based on trajectory modeling. In the same period, other biomass burning gases such as C_2H_6 also show an enhancement in their total column amounts which is highly correlated with the increase of the CO total columns. The observed total column values for CO are consistent with correlative data from MOPITT (Measurements Of Pollution In The Troposphere). Comparisons between our ground-based FTIR observations and space-borne observations from ACE-FTS (Atmospheric Chemistry Experiment – Fourier Transform Spectrometer) and HALOE (Halogen Occultation Experiment) confirm the feasibility of the FTIR measurements at Ile de La Réunion.

EGU

1 Introduction

The Network for the Detection of Atmospheric Composition Change[1] (NDACC, http://www.ndacc.org/) is a worldwide network of observatories, for which primary objectives are to monitor the evolution of the atmospheric composition and structure, and
5 to provide independent data for the validation of numerical models of the atmosphere and of satellite data. NDACC also supports field campaigns focusing on specific processes at various latitudes and seasons. Only a few stations in NDACC are situated in the tropical and subtropical belts. One of them is the Observatoire de Physique de l'Atmosphère de La Réunion (OPAR) (Baray et al., 2006), which is a measurement sta-
10 tion led by the Laboratoire de l'Atmosphère et des Cyclones (LACy) of the Université de La Réunion. It is located at 21°S, 55°E, in the Indian Ocean, East of Madagascar, at the edge between the southern tropics and subtropics. Although this station performs radio sonde observations since 1992, SAOZ measurements since 1993 and lidar measurements since 1994, it does not include the full suite of NDACC instruments, giving
15 a fairly incomplete picture of the atmospheric composition at this location. The implementation of Fourier transform infrared (FTIR) solar absorption measurements at Ile de La Réunion will partly fill the gap of observations in the southern hemisphere tropical region, as this technique provides information about the total column abundances and vertical distributions of a large number of atmospheric constituents (e.g., Brown et al.,
20 1992). To initiate long-term FTIR monitoring at Ile de La Réunion, we have performed two campaigns, one in 2002, and a second one in 2004. The first campaign served to demonstrate the feasibility of this type of measurements at this location, and the second one was held to provide data for satellite validation and to prepare for long-term monitoring by the time that a specific infrastructure for NDACC observations will become
25 available (planned for 2010). Comparisons with varous correlative data sets confirm the quality of the ground-based FTIR campaign data. In particular, the campaign in 2004 was set up to support the validation of the Atmospheric Chemistry Experiment –

---

[1]This was formerly called the Network for the Detection of Stratospheric Change or NDSC.

Ground-based FTIR measurements at Ile de La Réunion

C. Senten et al.

EGU

Fourier Transform Spectrometer (ACE-FTS), onboard the Canadian satellite SCISAT-1 (http://www.ace.uwaterloo.ca), launched in August 2003. Therefore, we include some comparisons between the ground-based FTIR and ACE-FTS overpass data in this paper. More information about the ACE mission, the ACE-FTS data, and the contribution of our FTIR campaign measurements at Ile de La Réunion to the validation of ACE-FTS can be found in Bernath et al. (2005), Boone et al. (2005), and several papers in the ACP ACE Validation Special Issue, respectively. A third FTIR campaign has started in May 2007 to run until December 2007, in order to extend the data set.

The results from the first and second campaign presented here concern a number of species that have been selected for three main reasons: their important roles in tropospheric or stratospheric chemistry, their link to current environmental problems, like climate change or stratospheric ozone depletion, and the fact that they are measured by ACE-FTS and other satellite experiments. More specifically, our analyses focus on the primary greenhouse gases CH_4, N_2O and O_3, on the secondary greenhouse gases CO and C_2H_6, and on HCl, HF and HNO_3. Apart from their indirect effect on climate change, CO and C_2H_6 play a central role in tropospheric chemistry through their reactions with the hydroxyl radical OH (Brasseur and Solomon, 1984). They are emitted primarily by anthropogenic sources, and they can be used as tracers of tropospheric pollution and transport (e.g., transport of emissions from biomass burning), because they have relatively high tropospheric abundances and long tropospheric lifetimes. In the stratosphere, HCl has a non-negligible impact on the ozone budget, acting as a reservoir species for chlorine. HF is a useful tracer of vertical transport, and of the anthropogenic emissions of fluorinated compounds. HNO_3 is formed in the reaction of OH with NO_2 and plays an essential role as a reservoir molecule for both the NO_x (nitrogen oxides) and HO_x (hydrogen oxides) radicals, which are potentially active contributors to the ozone destruction in the stratosphere through catalytic reactions.

In Sect. 2 and 3 we describe the campaign characteristics, the retrieval method and associated error budget evaluations. For every selected molecule individually, Sect. 4 discusses the optimal retrieval parameters and results, together with the error analysis.
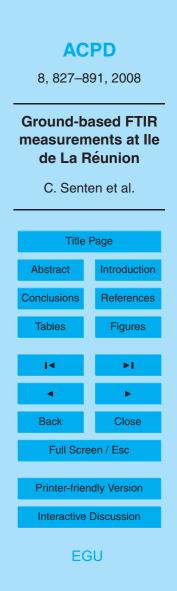
Ground-based FTIR measurements at Ile de La Réunion

C. Senten et al.

Full Screen / Esc

Printer-friendly Version

Interactive Discussion

EGU

Section 5 presents the methodology for comparison with correlative data and the thus obtained comparison results. Conclusions and future plans are given in Sect. 6.

2 Specifications of the FTIR measurement campaigns

During the first FTIR solar absorption measurement campaign at Ile de La Réunion, in October 2002, two almost identical instruments, i.e. mobile Bruker 120M Fourier Transform spectrometers, were operated in parallel at two different locations. The one belonging to the Belgian Institute for Space Aeronomy (BIRA-IASB) was installed on the summit of the mount Maïdo (2203 m a.s.l., 21°04′ S and 55°23′ E), and the one from the Université Libre de Bruxelles (ULB) at the nearby St-Denis University campus (50 m a.s.l., 20°54′ S and 55°29′ E). The BIRA-IASB instrument was placed in an air-conditioned container, and the electricity was provided with a power generator located south of the container. The solar tracker (purchased from Bruker) was mounted on a mast attached to the wall of the container, and the solar beam entered the container through a hole in that wall. The ULB instrument was installed in a laboratory of the university. Its solar tracker (also purchased from Bruker) was attached to the edge of the roof of the laboratory and the solar beam entered the room through a side-window.

During the second campaign, from August to October 2004, we limited ourselves to one instrument from BIRA-IASB at St-Denis only. The instrument was installed in the same container as in 2002, now put on the roof of a university building, with electricity provided by the university network. A different solar tracker was used, built at the University of Denver and modified at BIRA-IASB (Hawat et al., 2003; Neefs et al., 2007). In 2002 as well as in 2004, a second mast was used to carry a small meteorological station that belongs to the BARCOS system. BARCOS is the Bruker Automation and Remote COntrol System developed at BIRA-IASB to operate the FTIR experiment in an automatic or remotely controlled way (Neefs et al., 2007). It has been used successfully during both campaigns with the BIRA-IASB instrument. The BARCOS system includes a meteorological station and a data logger to continuously monitor and log

the local weather conditions as well as other housekeeping parameters, i.e. instrument and environment status. BARCOS executes a daily script that schedules and runs the measurements. It interrupts the observation schedule when the solar tracker is not capable of tracking the sun because of the presence of clouds, and it resumes the schedule once the sun re-appears. BARCOS automatically closes or opens the sun-tracker hatch when it starts or stops raining, respectively. Unfortunately, at the time of the campaigns, the automatic filling of the detector dewars with liquid nitrogen was not implemented yet, and hence it was not possible to operate the FTIR instrument without a person on site. Both spectrometers allowed a maximum optical path difference (MOPD) of 250 cm, providing a maximum spectral resolution, defined as 0.9/MOPD, of $0.0036\,cm^{-1}$. The high resolution solar absorption FTIR spectra were recorded using a KBr beamsplitter in the interferometer, and one of five different optical bandpass filters in front of the detector, which is a nitrogen-cooled InSb (indium antimonide) or MCT (mercury cadmium telluride or HgCdTe) detector, according to the target spectral range. The optical filters are the ones used generally in the NDACC FTIR community. The total spectral domain thus covered by our measurements spans the wavenumber range from 600 to $4300\,cm^{-1}$, in which it is possible to detect, among many other gases, the target species O_3, CH_4, N_2O, CO, C_2H_6, HCl, HF and HNO_3. Figure 1 shows composite spectra from the first campaign in 2002, at Maïdo and at St-Denis, including the different optical bandpasses (shown in different colours). For this figure, we selected spectra that were recorded on corresponding days for both locations and at solar zenith angles between 40° and 50°. All spectra have been standardized to improve the visibility of the figure. Note that some of the main absorbers are marked in the figure. One clearly observes the reduced absorptions by water vapour at the high altitude site of Maïdo. For example, the spectral range between 3000 and $3550\,cm^{-1}$, that is completely opaque at St-Denis, can be exploited at Maïdo. It must also be noted that during the 2002 campaign the spectral region between 1400 and $2400\,cm^{-1}$ has been covered using the MCT detector with a bandpass filter in the range 1350–2250 cm^{-1} (the so-called NDSC-5 filter). To improve the signal-to-noise ratio (SNR) in this

Ground-based FTIR measurements at Ile de La Réunion

C. Senten et al.

EGU

spectral region during the 2004 campaign, it was recorded with the InSb detector and the NDSC-4 filter (range 1850–2750 cm^{-1}). This change in measurement configuration has an impact on the quality of the CO data, as will be seen in Sect. 4.4. Whenever the sky was clear at local noon, a reference HBr cell spectrum was recorded using
5   the NDSC-4 filter. For this purpose, a cell containing hydrogen bromide (HBr) at low pressure (2 mbar) was placed in the interferometer output beam in front of the InSb detector, and a spectrum was recorded using the sun as light source. When this was not possible on several consecutive days because of the noontime weather situation, the reference HBr cell spectrum was taken the same way, but using a tungsten lamp
10 source. The cell spectra have been analysed using Linefit version 8 (Hase et al., 1999), to monitor the alignment of the instrument. For the ULB instrument at St-Denis, a cell spectrum was taken only once during the first campaign; it confirmed the correct alignment of the instrument. Because reliable solar absorption measurements require clear sky conditions, the number of observation days was limited: in total, we had about
15 24 days with observations during the first campaign and about 60 days during the second campaign. Also, during the first campaign, it was often not possible to perform the measurements simultaneously at both sites, because the local weather conditions were not necessarily the same. It is worth mentioning that most of the measurements have been carried out before noon, because most often clouds appeared in the afternoon.
20 Sometimes additional late evening measurements have been possible at Maïdo.

3   General description of the retrieval method and error budget evaluation

As already mentioned, we have focused on the retrieval of ozone (O_3), methane (CH_4), nitrous oxide (N_2O), carbon monoxide (CO), ethane (C_2H_6), hydrogen chloride (HCl), hydrogen fluoride (HF) and nitric acid (HNO_3). In addition to the total column abun-
25 dances of these molecules, we have extracted information – whenever feasible – about their vertical distribution in the altitude range where the pressure broadening of the absorption lines can be resolved. For these retrievals, we have used the inversion

Ground-based FTIR measurements at Ile de La Réunion
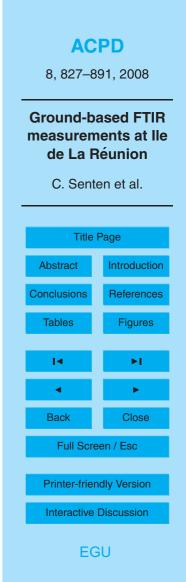
C. Senten et al.

EGU

algorithm SFIT2 (v3.92), jointly developed at the NASA Langley Research Center, the National Center for Atmospheric Research (NCAR) and the National Institute of Water and Atmosphere Research (NIWA) at Lauder, New Zealand (Rinsland et al., 1998). This algorithm uses a semi-empirical implementation of the Optimal Estimation Method (OEM) of Rodgers (2000). Further details on the SFIT2 program can be found in the paper by Hase et al. (2004).

All retrievals are executed on a 44 layer altitude grid, starting at 50 m a.s.l. for St-Denis and at 2200 m a.s.l. for Maïdo, with layer thicknesses of about 1.2 km in the troposphere and lower stratosphere up to 33.4 km altitude, then growing steadily to about 4 km around 50 km altitude and to about 8 km for the higher atmospheric layers up to 100 km. This choice was made to take into account the local atmospheric pressure and temperature variabilities. Daily pressure and temperature profiles were taken from the National Centre for Environmental Prediction (NCEP). For the error analysis (see Sect. 3.4.3) we also used temperature profiles from the European Center for Medium range Weather Forecasting (ECMWF).

3.1 Forward model parameters

The forward model in SFIT2 is a multi-layer multi-species line-by-line radiative transfer model. The instrument parameters in the forward model include a wavenumber scale multiplier and background curve parameters, as well as the actual optical path difference (OPD) and field of view (FOV) of the instrument. The background slope and curvature are determined by fitting a polynomial of degree 2, and the wavelength shift is also fitted in every spectral micro-window independently. To account for deviations from the ideal instrument lineshape function (ILS) due to small instrument misalignments or imperfections, apodization and phase error functions are included. These functions can either be acquired from the Linefit analyses of the measured HBr cell spectra, or they can be approximated by a polynomial or a Fourier series of a user specified order. Our retrievals have been carried out using the second approach, i.e. fitted empirical apodization and phase error functions, because in all our retrievals this

Ground-based FTIR measurements at Ile de La Réunion

C. Senten et al.

EGU

approach resulted in the smallest spectral residuals and the least oscillations in the retrieved profiles. In particular, we approximated the empirical apodization by a polynomial of degree 2 and, if beneficial, the empirical phase error by a polynomial of degree 1.

3.2 Inverse model

The inverse problem consists of determining the state of the atmosphere, in particular the vertical distributions of the target molecules, from the observed absorption spectra. In order to solve this ill-posed problem, the SFIT2 retrievals request ad hoc covariance matrices for the uncertainties associated with the a priori vertical profiles of the target gases and with the measurements. The retrieved profiles and total column amounts of the target species are the ones that provide the best representation of the truth, given the measurements and the a priori information, and their respective uncertainties.

3.2.1 A priori profile and associated covariance matrix

The used a priori profile $\mathbf{x}_a$ and its covariance matrix $\mathbf{S}_a$ should well represent a first guess of the "true" state, in order to reasonably constrain the retrieval solution, in particular at those altitudes where one can hardly get information out of the measurements. For each target gas we have decided to use one single a priori profile and associated covariance matrix for both campaigns, to avoid any biases between the results and to make sure that the results are directly comparable. The diagonal and off-diagonal elements of each $\mathbf{S}_a$ have been chosen such as to yield the best compromise between the spectral residuals, the number of oscillations in the retrieved profiles, and the number of degrees of freedom for signal (DOFS; see Sect. 3.3). We have assumed that correlations between layers (i.e. off-diagonal elements) decay according to a Gaussian-shaped function. Details about the choice of the a priori vertical profiles and the associated covariance matrices are provided for each molecule individually in Sect. 4. While we used constant values on the diagonal of $\mathbf{S}_a$ for the retrievals of all

molecules, except CH_4, we used more realistic uncertainties in the error calculations. Nevertheless, the $\mathbf{S}_a$ matrices used in the error analysis still have a Gaussian shape because of the limited knowledge about their full structure.

3.2.2 Measurement noise covariance matrix

The covariance matrix associated with the measurements, $\mathbf{S}_\varepsilon$, is considered to be diagonal, containing an ad hoc estimation of the squared reciprocals of the SNR of the observed spectra as diagonal elements. Together with the a priori covariance matrix of the profiles, the measurement noise covariance matrix has a great influence on the retrieval characterization and error analysis, as will be discussed in Sect. 3.4.

3.2.3 Selection of spectral micro-windows

Deriving information about the vertical distribution of trace gases out of high resolution FTIR spectra is possible because of the pressure broadening of the absorption lines, leading to an altitude dependence of the line shapes. While the line centers provide information about the higher altitudes of the distribution, the wings of a line provide information about the lower altitudes. Therefore the information content of the retrieval will strongly depend on the choice of the absorption lines. For all species, the absorption line parameters were taken from the HITRAN 2004 spectral database (Rothman et al., 2005). In addition, updates for H_2O, N_2O, HNO_3 and C_2H_6 line parameters that are available on the HITRAN site (http://www.hitran.com) have been included. We have verified that they give similar or slightly better spectral fits than the original HITRAN 2004 values. The retrieval spectral micro-windows are selected such that they contain unsaturated well-isolated absorption features of the target species with a minimal number of interfering molecular lines. One also aims at maximizing the amount of information present in the spectra, represented by the DOFS. For the present retrievals, we adopted spectral micro-windows used by other FTIR research groups and we verified slight modifications of those micro-windows, in order to improve our retrievals.

EGU

Further details about the micro-window selections and characteristics are discussed in Sect. 4.

3.3 Information content and sensitivity

The retrieved state vector $\mathbf{x}_r$ is related to the a priori and the true state vectors $\mathbf{x}_a$ and $\mathbf{x}$, respectively, by the equation (Rodgers, 2000):

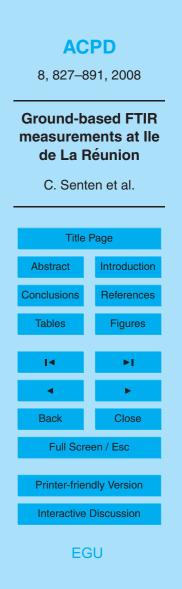$$\mathbf{x}_r = \mathbf{x}_a + \mathbf{A}(\mathbf{x} - \mathbf{x}_a). \tag{1}$$

The rows of the matrix $\mathbf{A}$ are called the averaging kernels and the trace of $\mathbf{A}$ equals the DOFS. For each of the 44 layers the full width at half maximum of the averaging kernels provides an estimate of the vertical resolution of the profile retrieval at the corresponding altitude, while the area of the averaging kernel represents the sensitivity of the retrieval at the corresponding altitude to the true state. The DOFS together with the averaging kernel shapes, will define the partial columns that best represent the retrieval results. The error analysis has been carried out for these partial columns.

3.4 Error analysis

Using the formalism described in Rodgers (2000) – assuming a linearization of the forward and inverse model about some reference state and spectrum respectively – the difference between the retrieved and the real state of the atmosphere can be written as:

$$\mathbf{x}_r - \mathbf{x} = (\mathbf{A} - \mathbf{I})(\mathbf{x} - \mathbf{x}_a) + \mathbf{G}_y \mathbf{K}_b (\mathbf{b} - \mathbf{b}_r) + \mathbf{G}_y (\mathbf{y} - \mathbf{y}_r), \tag{2}$$

where $\mathbf{A}$ is the averaging kernel matrix as defined in Sect. 3.3, $\mathbf{I}$ the identity matrix, $\mathbf{G}_y$ the gain matrix representing the sensitivity of the retrieved parameters to the measurement, $\mathbf{K}_b$ the sensitivity matrix of the spectrum to the forward model parameters $\mathbf{b}$, $\mathbf{b}_r$ the estimated model parameters, $\mathbf{y}$ the observed spectrum, and $\mathbf{y}_r$ the calculated spectrum. The equation above splits the total error in the retrieved profile into three different

EGU

error sources, i.e. the smoothing error, the forward model parameter error including the temperature error, and the measurement error. Besides these random errors we must also consider the systematic errors due to uncertainties in the spectroscopic line parameters. More details about the evaluation of the individual contributions to the error budget are provided in the next sections.

3.4.1 Smoothing error

The smoothing error covariance is calculated as $(\mathbf{I}-\mathbf{A})\mathbf{S}_a(\mathbf{I}-\mathbf{A})^t$, where $\mathbf{S}_a$ is the a priori covariance matrix (see Sect. 3.2.1). In order to construct a realistic $\mathbf{S}_a$ matrix, we need information about the variability and covariances of an ensemble of real profiles. However, this information is not always available at all altitudes, obliging us to replace $\mathbf{S}_a$ with a Gaussian covariance matrix for example, for which we still have to estimate the natural variabilities and the inter-layer correlations based on real data. We have chosen these values such that $\mathbf{S}_a$ approaches the covariance matrix derived from satellite measurements. For the construction of the a priori covariance matrix for each species we calculated the weighted covariance matrix of all available vertical profiles measured by the specified satellite within the 15° longitude and 10° latitude rectangle around Ile de La Réunion, and used the resulting diagonal elements to create $\mathbf{S}_a$. The thus obtained variabilities that are reliable within a certain altitude range are then extrapolated to the complete altitude range (0–100 km) by repeating the lower- and uppermost value. The off-diagonal elements of $\mathbf{S}_a$ are defined by a Gaussian distribution having a HWHM which can be different for each molecule. Table 1 summarizes the satellite used for every trace gas, the altitude range in which they provide reliable values and the HWHM used to calculate the Gaussian off-diagonal elements of the $\mathbf{S}_a$ matrix. For more information about the satellite data used, we refer to Sect. 5. Figure 2 shows the resulting uncertainties in the a priori volume mixing ratios of each species as a function of altitude.

Ground-based FTIR measurements at Ile de La Réunion

C. Senten et al.

3.4.2 Forward model parameter error

We considered the random uncertainties in the forward model parameters, described in Sect. 3.1, to be mutually independent; hence we used a matrix $\mathbf{S}_b$ that is diagonal. For the wavenumber shift, background curve parameters, and ILS parameters, we adopted uncertainties of 10%, 10%, and 20%, respectively. We also included in $\mathbf{S}_b$ the uncertainties on the total column amounts of the interfering species: they have been estimated by computing the standard deviations of the fitted column values. The resulting errors on the retrieved target profile are then calculated as $(\mathbf{G}_y\mathbf{K}_b)\mathbf{S}_b(\mathbf{G}_y\mathbf{K}_b)^t$.

3.4.3 Temperature error

The atmospheric temperature profile is a forward model parameter that is not fitted. Nevertheless, the associated uncertainties must be considered as well, because they influence the uncertainties on the retrieved profiles via the temperature dependence of the absorption lines. The temperature error covariance matrix is calculated as $(\mathbf{G}_y\mathbf{K}_T)\mathbf{S}_T(\mathbf{G}_y\mathbf{K}_T)^t$, in which $\mathbf{S}_T$ is a realistic covariance matrix of the temperature profile uncertainties. The factor $(\mathbf{G}_y\mathbf{K}_T)$, i.e. the partial derivative of the retrieval to the temperature, has been determined by repeating the retrieval with a slightly perturbed temperature profile. Our estimation of $\mathbf{S}_T$ is based on the differences between the NCEP and ECMWF temperature profiles calculated for Ile de La Réunion in the period August–October, 2004. This matrix is visualized in Fig. 3. The 41 layers from high to low altitude are defined as follows: from 100 to 50 km by steps of 5 km, from 50 to 10 km by steps of 2 km and from 10 km to the surface by steps of 1 km. As the NCEP profiles do not reach higher than about 54 km, we have repeated the covariances at 50 km for all altitudes above.

Ground-based FTIR measurements at Ile de La Réunion

C. Senten et al.

Title Page

Abstract | Introduction

Conclusions | References

Tables | Figures

|◄ | ►|

◄ | ►

Back | Close

Full Screen / Esc

Printer-friendly Version

Interactive Discussion

EGU

3.4.4 Measurement error

The uncertainties coming from the measurement noise are calculated as $\mathbf{G}_y \mathbf{S}_\varepsilon \mathbf{G}_y^t$, where $\mathbf{S}_\varepsilon$ is the measurement noise covariance matrix as defined in Sect. 3.2.2. While the SNR used for the retrievals was an ad hoc estimation of the true SNR, we used more realistic SNR values for the error calculations. These values have been determined by dividing the largest signal of the target molecule in the selected micro-window(s) by the root mean squared (rms) value of the differences between the observed and calculated spectrum.

3.4.5 Line intensity and pressure broadening error

In addition to the random error budget, we determined the systematic error in the retrievals originating from the uncertainties in the spectroscopic line intensities and in the pressure broadening coefficients. We therefore perturbed the spectroscopic line intensities and broadening coefficients, respectively, of the target lines within our micro-windows, by their maximum uncertainties as given by Rothman et al. (2005). The corresponding full systematic error covariance matrices are then calculated based on the differences between the thus retrieved vertical profiles and the original retrieved profile.

4 Retrieval results and error budgets

In this section, we give an overview of our retrieval approach for all target molecules, followed by a discussion of the results obtained and of the error budget per molecule.

The micro-windows in which O_3, CH_4, N_2O, CO and C_2H_6 are retrieved, as well as the interfering absorbers whose total columns are fitted simultaneously with the target species, have been adopted from the EC project UFTIR (http://www.nilu.no/uftir; De Mazière et al., 2004). Our tests have shown that these windows are still appropriate for

the Maïdo and St-Denis sites at Ile de La Réunion, despite the prevailing high humidity. The UFTIR project also provided us with corrected spectral line parameters for ozone in the 2960–2980 cm^{-1} region (D. Mondelain and A. Barbe, private communication). The implementation of these corrections improves the spectral fits for C_2H_6, compared to when we used the O_3 line parameters from the HITRAN 2004 catalogue. For HF and HCl the fitted micro-windows and interfering species were adopted from Reisinger et al. (1994) and from Rinsland et al. (2003), respectively. The HNO_3 micro-window is based on the discussions by Flaud et al. (2006) and Perrin et al. (2004). Table 2 gives a summary of the optimal choice of the diagonal elements and the half-width at half-maximum (HWHM) defining the Gaussian inter-layer correlation length of **S**$_a$ adopted in the retrieval, the retrieval micro-windows fitted simultaneously, the spectral resolution, the effective SNR, the associated interfering molecules, and the achieved mean DOFS, at Maïdo, 2002, and St-Denis, 2002 and 2004, for each target species retrieved from both campaigns. Figure 4 shows the resulting time series of the retrieved total column amounts (in molecules/cm^2) of all species at St-Denis in 2002 and 2004. The results of the error calculations for representative Maïdo and St-Denis spectra, recorded at solar zenith angles between 40° and 65°, are summarized in Tables 3 and 4, respectively; note that we only show the error values for the 2004 campaign at St-Denis, because the 2002 campaign yields similar values for this location. It is clear from Tables 3 and 4 that it depends on the target species which one of the various contributions to the overall error budget is the dominant one. The temperature error is more important when the lower state energies of the absorbing lines in the micro-windows become higher, which is the case for example for some CH_4 and O_3 lines. The smoothing error is larger when the DOFS is smaller and when the true profile has more vertical structure, confirming that there is less vertical information in the retrieval. If the DOFS exceeds one, the smoothing error is larger for the independent partial columns than it is for the total column. The smoothing error is highest for the partial columns in which the species' profile has more vertical structure. The measurement error, due to our definition of true SNR, becomes very large for weakly absorbing target species
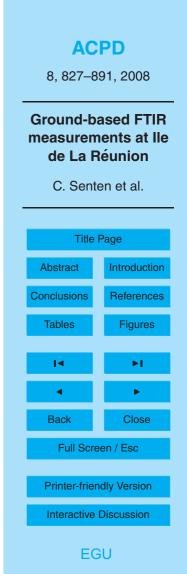
Ground-based FTIR measurements at Ile de La Réunion

C. Senten et al.

EGU

(e.g., C_2H_6), and for target absorption lines sitting on the wing of a strong absorbing interfering species (e.g., HF). The measurement error for CO at Maïdo in 2002 was unusually high, because of a less appropriate choice of optical filter and detector for the observation of the spectral range in which the CO micro-windows are located,

5 as mentioned before (see Sect. 2). The systematic error budget uncertainties are especially high for CH_4, because of strong uncertainties in the CH_4 spectroscopy. From a comparison of Tables 3 and 4, we see that both the random and systematic errors depend to some extent on the altitude of the observatory. This can be understood partly by the fact that the strength of the interferences with water vapour absorptions

10 change drastically between the high-altitude Maïdo site and the site of St-Denis which is near to sea-level.

4.1 Ozone (O_3)

For the O_3 retrievals, we adopted a single mean a priori profile from the UGAMP (UK Universities Global Atmospheric Modelling Programme,

15 http://ugamp.nerc.ac.uk/) climatology, calculated for a square of 2.5°×2.5° enclosing St-Denis (http://badc.nerc.ac.uk/data/ugamp-o3-climatology/), which provides a global 4D climatological distribution of ozone covering the years 1985 to 1989.

Figure 5 shows the single micro-window fit of O_3 from a single spectrum on 13 October 2002 and 15 October 2004 at Maïdo and St-Denis, respectively, together with the

20 residuals, computed as measured minus simulated transmission. In the spectral fits for St-Denis we observe systematic residuals around 1001.10 and 1003.70 cm^{-1}, which are due to water vapour lines. However, fitting H_2O profiles first to use the resulting daily a priori profiles in the O_3 retrieval, or excluding the two small regions from our micro-window, did not affect the retrievals significantly. We obtain about 5 DOFS for

25 O_3 at both sites. It is therefore possible to distinguish 5 independent layers with good sensitivity, namely 2 layers in the troposphere (0.1 to 8.2 and 8.2 to 17.8 km), and 3 layers in the stratosphere (17.8 to 23.8, 23.8 to 31.0 and 31.0 to 100 km). For both sites the measurement error is the dominant error source on the partial columns (see
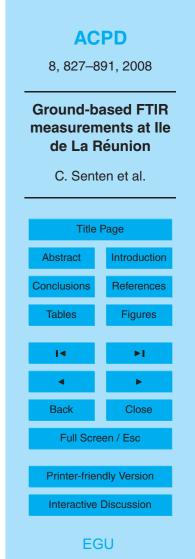
Tables 3 and 4), whereas the temperature error has the largest contribution to the total column error.

4.2 Methane (CH_4)

The CH_4 a priori profile was based on available data from the Halogen Occultation Experiment (HALOE), onboard the Upper Atmosphere Research Satellite (UARS), launched in September 1991 (http://haloedata.larc.nasa.gov/home). CH_4 retrievals from HALOE have been validated by Park et al. (1996). We took a six year mean of all HALOE (version 19) vertical profiles from 2000 to 2005 within the 15° longitude and 10° latitude rectangle around Ile de La Réunion. The resulting weighted mean profile covers the range 14 to 80 km, so below and above these altitudes we have extrapolated the profile by repeating the values at 14 and 80 km, respectively. In contrast to all other retrieved molecules we have used non constant diagonal elements to construct $\mathbf{S}_a$. These values are calculated out of the same HALOE profiles as used to determine the a priori profile. This is done, because it significantly reduces the large oscillations in the retrieved profiles that emerge when using constant uncertainties. The obtained variabilities from 14.2 to 78.4 km are then extrapolated to the complete altitude range by repeating the first and last value. The off-diagonal elements are defined by a Gaussian distribution having a HWHM of 6 km. This same covariance matrix is used for the error calculations.

Figure 6 shows the multiple micro-window fit of CH_4 from a single spectrum on 16 October 2002 and 12 October 2004 at Maïdo and St-Denis, respectively, together with the residuals, computed as measured minus simulated transmission. Note that the retrieved profiles slightly oscillate near the surface. As the number of DOFS is about 2 at both sites, we manage to resolve two independent partial columns of CH_4, namely 0.1 to 13.0 and 13.0 to 100 km. For the errors in the CH_4 total and partial columns, the same conclusion as for O_3 holds true, i.e. the measurement error dominates except for the total column for which the temperature error has a major contribution to the total random error.
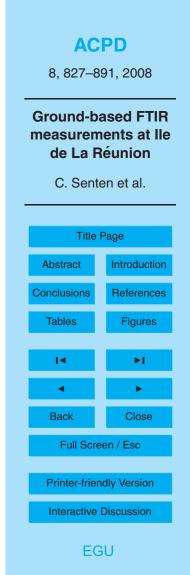
Ground-based FTIR measurements at Ile de La Réunion

C. Senten et al.

[EGU](#)

4.3 Nitrous oxide (N$_2$O)

For the N$_2$O a priori profile we used the 1976 U.S. Standard profile (U.S. NOAA, 1976) scaled with a yearly factor of 0.25%, to account for the slight yearly N$_2$O increase observed by Zander et al. (2005).

Figure 7 shows the multiple micro-window fit of N$_2$O from a single spectrum on 16 October 2002 and 12 October 2004 at Maïdo and St-Denis, respectively, together with the residuals, computed as measured minus simulated transmission. As the number of DOFS for N$_2$O is about 3 for Maïdo as well as for St-Denis, three independent partial columns can be distinguished, in particular from 0.1 to 4.6, from 4.6 to 15.4 and from 15.4 to 100 km. For N$_2$O at Maïdo and St-Denis the smoothing error has the largest contribution to the total random error, for the total column as well as for the partial columns.

4.4 Carbon monoxide (CO)

The CO a priori profile has been based on available data from the MOPITT space-borne instrument. CO retrievals from MOPITT have been validated by Emmons et al. (2004). Our CO a priori profile is a five year mean of all MOPITT vertical profiles (version L2V5) from 2000 to 2004 within 15° longitude and 10° latitude around the location of our observations. We only used daytime measurements for which the solar zenith angle was smaller than 80°. The thus obtained mean a priori profile from 0 to 14 km was then completed with the U.S. Standard Atmosphere (1976) values from 16 to 100 km.

Figure 8 shows the multiple micro-window fit of CO from a single spectrum on 19 October 2002 and 12 October 2004 at Maïdo and St-Denis, respectively, together with the residuals, computed as measured minus simulated transmission. A large measurement noise was found for the spectral data from 2002 at Maïdo, especially in the 2157.40–2159.35 cm^{-1} window. This is due to the fact that this window is situated in the tail of the spectral range of the bandpass filter used at that time to cover this region, as

Ground-based FTIR measurements at Ile de La Réunion

C. Senten et al.

Title Page

Abstract | Introduction

Conclusions | References

Tables | Figures

◄ | ►

◄ | ►

Back | Close

Full Screen / Esc
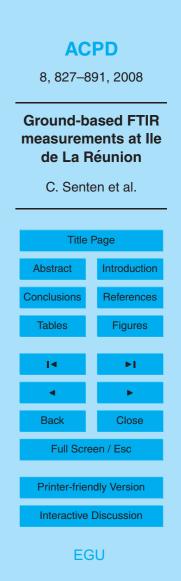
Printer-friendly Version

Interactive Discussion

EGU

explained in Sect. 2. It induces a large uncertainty in the retrieval results, as is obvious in Table 3. This problem was solved in 2004 by using another bandpass filter. The DOFS for CO in our measurements is about 2.7, providing us with just 2 independent layers, namely 0.1 to 13.0 and 13.0 to 100 km. For CO clearly the measurement error dominates over all other error sources. This is due to the limited SNR within our fitted micro-windows.

We compared the retrieved CO total columns with data from the Measurements Of Pollution In The Troposphere (MOPITT) instrument on-board the EOS-TERRA satellite, which was launched in December 1999 (http://terra.nasa.gov/About/MOPITT/index.php). Figure 9 shows the CO partial and total columns above Ile de La Réunion obtained from our ground-based FTIR measurements during the campaign in 2004, together with the correlative total columns from MOPITT. It also includes the relative differences between both data sets for coinciding dates, defined as $100^*(TC_{FTIR}-TC_{MOP})/TC_{MOP}$. We observe a very good agreement between the time series – both showing the seasonal trend of CO – although MOPITT seems to slightly overestimate the CO concentrations – and an additional increase around 12 October. The mean relative difference between the corresponding FTIR and MOPITT total column values is -10.6%. A similar bias was also noticed by Barret et al. (2003) and Emmons et al. (2004). The observed enhancement of the CO tropospheric concentrations by the end of October 2004 agrees with the known seasonal cycle of CO in the southern tropical and subtropical regions, which is attributed to the effect of enhanced mean biomass burning and cross-equatorial transport of CO from the northern hemisphere (WMO WDCGG, 2006). The additional increase for a few days around 12 October originates from fire emissions in southern Africa and Madagascar.

In order to establish a clear source-receptor relationship between the FTIR site at St-Denis and potential gas emitting locations, retroplumes were calculated using the Lagrangian particle dispersion model FLEXPART, version 6.2 (Stohl et al., 1998, 2005). This model simulates the transport and dispersion of linear tracers, by calculating the

Ground-based FTIR measurements at Ile de La Réunion

C. Senten et al.

Title Page

Abstract | Introduction

Conclusions | References

Tables | Figures

|◄ | ►|

◄ | ►

Back | Close

Full Screen / Esc

Printer-friendly Version

Interactive Discussion

EGU

trajectories of a chosen multitude of particles. Not only do the retroplumes trace the origin of a particular air mass, they also give an estimate on the amount of time the air mass has spent in close proximity to the Earth's surface. Knowledge of this residence time can deliver insight into the trace gas emitted versus detected ratio. The model was

5 driven by global wind field data from ECMWF, with a spatial resolution of 1°×1° and 60 vertical levels and a temporal resolution of 3 h. The fire emissions used are 8 day averages taken from the Global Fire Emissions Database (GFED), version 2 (Van der Werf et al., 2006), using MODIS fire hot spots (Giglio et al., 2003). The emissions were distributed as follows: 20% between 0–100 m altitude, 40% between 100–500 m and 40%

10 between 500–1000 m. Anthropogenic CO emissions, which have a small contribution, were taken from the EDGAR 3.2 Fast Track 2000 database (http://www.mnp.nl/edgar). Background CO was fixed at 85 ppb, since this is the lowest CO amount between 1 and 13 km, observed by FTIR in the period September–October 2004. Note that this could well be an underestimation, as background CO levels are increasing in this period. For

15 our calculations we released 200 000 particles between 0 and 13 km over St-Denis for each corresponding FTIR measurement. Each release lasted for 602 s and each CO retroplume was traced back in time for 20 days. For each retroplume, its residence time near the surface has been calculated (in $s\,m^3\,kg^{-1}$). If this response function is folded with the 3D field of emission flux data (in $kg\,m^{-3}\,s^{-1}$) into this grid box, a mass

20 mixing ratio at the receptor point is obtained. Figure 10 shows time series of such CO abundances between 0 and 13 km altitude at Ile de La Réunion in October 2004, measured by ground-based FTIR and calculated by FLEXPART. One can clearly see an enhancement in the CO amounts around 12 October, although much more obvious in the FTIR time series than in the FLEXPART series. This increase can be attributed to

25 the transport of CO amounts originating from biomass burning events in Madagascar and southern Africa the days before, as confirmed by Fig. 11, showing the total CO amounts emitted and transported to Ile de La Réunion on 12 October. In order to obtain in the FLEXPART simulations the same CO levels as the observed ones, we had to increase the GFED emissions by a factor of 4; the corresponding time series are also

EGU

shown in Fig. 10. One must not forget however that there are quite some uncertainties in the fire emissions due to their high variability. Other factors that could lead to the observed differences between the FLEXPART simulations and the ground-based FTIR observations are: (1) we have traced back the emissions to 20 days, while the lifetime of CO permits contributions from larger time frames, (2) there are still non negligible errors in the wind fields, especially in their vertical component, (3) the temporal emission resolution (8 day averages) is not very accurate, and (4) the choice of the vertical distribution of the emissions up to 1 km is rather arbitrary since in reality the altitude dependence of the emissions is strongly influenced by the size, temperature, and type of fire (e.g., Hyer et al., 2007).

4.5 Ethane (C_2H_6)

Between 12 and 30 km, the a priori profile for C_2H_6 was adopted from Cronn and Robinson (1979) and above 30 km from Rudolph and Ehhalt (1981). Below 12 km the a priori volume mixing ratio was set constant at 7×10^{-10} ppv.

Figure 12 shows the single micro-window fit of C_2H_6 from a single spectrum on 14 October 2002 and 9 October 2004 at Maïdo and St-Denis, respectively, together with the residuals, computed as measured minus simulated. Since we obtain about 1.6 DOFS, we consider only total column amounts of C_2H_6. Again uncertainties in the measured spectra are the largest error source. The time series of the total column values of C_2H_6 at St-Denis in 2004 shows an increase by the end of October, in line with the observed increase of the tropospheric CO amount (Fig. 9).

Figure 13 shows the correlation plot of CO total columns versus C_2H_6 total columns during the 2002 and 2004 campaigns at St-Denis. The correlation coefficient equals 0.91 (number of points is 42), confirming that the observed increases have the same origin, namely tropical biomass burning in Madagascar and on the African continent. Analogous results have been shown by Rinsland et al. (1998) and Zhao et al. (2002).

4.6 Hydrogen chloride (HCl)

The HCl a priori profile between 16 and 60 km was created from HALOE (version 19) observations, following the same approach as for CH_4. HCl retrievals from HALOE have been validated by Russell et al. (1996a). Below 16 km the profile was completed with values from Smith (1982) and above 60 km a constant mixing ratio was adopted, which was equal to the upper value of the weighted mean HALOE profile.

For the HCl retrievals Rinsland et al. (2003) propose to fit two other micro-windows around 2727.78 and 2775.78 cm^{-1}, in addition to the two windows we use. But since they contain strong interfering water vapour lines, fitting them appeared to be problematic at our (sub)tropical site. We therefore restricted our spectral fits to the two micro-windows defined above.

Figure 14 shows the multiple micro-window fit of HCl from a single spectrum on 16 October 2002 and 15 October 2004 at Maïdo and St-Denis, respectively, together with the residuals, computed as measured minus simulated transmission. Note that around 25 km the retrieved profile differs strongly from the a priori profile. Such deviations are observed for all our HCl measurements, but up to now we did not manage to find the origin of this structure. Again, we can only derive total column amounts, because the number of DOFS for HCl is about 1.3 at both sites. Also for HCl the measurement error is the largest random error on the total column.

4.7 Hydrogen fluoride (HF)

The HF a priori profile between 14 and 60 km was derived from HALOE (version 19) observations, as was done for HCl. HF retrievals from HALOE have been validated by Russell et al. (1996b). The profile was extrapolated with constant values above and below that altitude range, by repeating the volume mixing ratio at 60 and 14 km, respectively.

Figure 15 shows the single micro-window fit of HF from a single spectrum on 13 October 2002 and 11 October 2004 at Maïdo and St-Denis, respectively, together with

Title Page

Abstract | Introduction

Conclusions | References

Tables | Figures

◄ | ►

Back | Close

Full Screen / Esc

Printer-friendly Version

Interactive Discussion

EGU

the residuals, computed as measured minus simulated transmission. The 1.5 DOFS tell us that we can only determine the total columns of HF. Also for HF the measurement error is the largest random error on the total column. For Maïdo the measurement error dominates, whereas for St-Denis the smoothing error has the largest contribution to the total random error for the HF total columns.
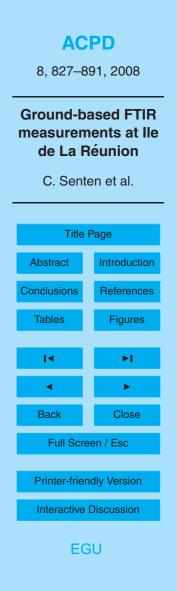
4.8 Nitric acid (HNO_3)

For the creation of an HNO_3 reference profile, we used data from the SMR instrument, onboard the satellite Odin, launched in February 2001 (http://diamond.rss.chalmers.se/Odin). HNO_3 retrievals from Odin have been validated by Urban et al. (2005). In particular, we calculated a five year mean, from 2001 to 2005, of all Odin/SMR profiles (version 2.0) within a 1500 km radius around St-Denis. This gave us representative a priori values between 16 and 36 km. Below and above these altitudes we completed the profile with a seasonal mean climatology for the 0°–20° S latitude band in the period September–November 2002 from the Michelson Interferometer for Passive Atmospheric Sounding (MIPAS) onboard ESA's Envisat satellite, launched in March 2002 (http://envisat.esa.int/instruments/mipas/index.html). HNO_3 retrievals from MIPAS have been validated by Oelhaf et al. (2004) and Wang et al. (2007).

Figure 16 shows the single micro-window fit of HNO_3 from a single spectrum on 16 October 2002 and 21 October 2004 at Maïdo and St-Denis, respectively, together with the residuals, computed as measured minus simulated transmission. For HNO_3 we get about 1 DOFS, so again only total column amounts can be obtained. Due to the small SNR in our fitted micro-window for HNO_3, again the measurement error dominates.

5 Comparisons with correlative data

5.1 Methodology

The retrieval results obtained from our ground-based FTIR measurements have been compared with correlative vertical profile or partial column data from complementary ground-based observations at the site or from satellites. If the correlative data have a higher vertical resolution than the FTIR data, they are smoothed with the FTIR averaging kernels, using the formula (Rodgers and Connor, 2003)

$$\mathbf{x}' = \mathbf{x}_a + \mathbf{A}(\mathbf{x} - \mathbf{x}_a). \tag{3}$$

For all comparisons with satellite data, we used coincidence criteria of maximum 15° difference in longitude, 10° in latitude, and maximum 24 h time difference. Besides the comparisons with ACE-FTS data as part of the ACE validation project, we have compared our FTIR observations with validated data from the HALOE satellite instrument. We have not found any other space-borne correlative data to compare with, knowing that MIPAS has stopped operating in nominal mode in March 2004. In addition to the comparisons with satellite observations, sonde measurements performed at Ile de La Réunion in the frame of the SHADOZ network (http://croc.gsfc.nasa.gov/shadoz/) are used to evaluate our FTIR data. Unfortunately, there are no correlative O_3 profiles from the lidar instrument at Ile de La Réunion, because the lidar was not operational during our measurement campaigns.

The comparisons between the ground-based FTIR and the correlative data are limited to comparisons between partial columns (PCs), defined by the altitude ranges in which the DOFS is close to or larger than one. In any case, the comparisons are restricted to the altitude ranges within which the sensitivity of the FTIR measurement, as defined in Sect. 3.3, is equal to or greater than 50%. We therefore define the relative difference between the ground-based FTIR and smoothed satellite data, PC_{SAT}, as $100^*(PC_{SAT}-PC_{FTIR})/PC_{FTIR}$, and analogously the relative difference between the ground-based FTIR and smoothed sonde data as $100^*(PC_{FTIR}-PC_{SONDE})/PC_{SONDE}$.

EGU

To support the interpretation of the observed differences between the FTIR and correlative partial column data, we have evaluated the random errors associated with the relative differences, from the combined errors of the FTIR and correlative sonde or satellite profiles. Note that the smoothing error contribution can be neglected in this evaluation, because we have first smoothed the higher vertical resolution profile from sonde or satellite (Rodgers and Connor, 2003).

5.2 FTIR versus ozone sonde

There are only four days during the second campaign on which O_3 soundings and FTIR measurements have both been carried out. These are 18 August, 1 and 16 September, and 4 October 2004. The vertical profiles agree well in the high sensitivity altitude range. As an example, Fig. 17 shows the comparison of the O_3 profiles on 16 September 2004. We observe a relative difference between the FTIR and smoothed sonde O_3 partial column amounts in the altitude range where both measurements are sensitive, i.e. in this case from the surface to 31 km altitude, of about 8%. The comparison results for all four days are summarized in Table 5, together with the number of DOFS for the partial column in the considered altitude range, and the percentage random error associated with the relative difference, from the combined sonde and FTIR random errors. Since the random error budget for the ozone sondes was not given in the NDACC database, we used typical values from the JOSIE-2000 report (Smit and Straeter, 2004): 5% from the ground up to 20 km, and 7% above. From Table 5, we deduce that the ground-based FTIR retrievals overestimate the amount of O_3 between the surface and 30 km by 0% to 8%; of course, this conclusion is based on only 4 coincidences.

5.3 FTIR versus ACE-FTS

During the 2004 campaign, there have been five overpasses of ACE above the Ile de La Réunion: occultation sr5497 on 20 August, occultation ss6153 on 3 October,

occultation ss6168 on 4 October, occultation ss6197 on 6 October, and occultation sr6485 on 26 October. For each of these occultations, we have compared the ground-based FTIR data with the ACE-FTS profiles (version v2.2). Note that the profiles measured by the ACE-FTS occultation on 26 October do not reach altitudes below 16.6 km.

⁵ Therefore the resulting comparisons for that day are not very valuable, but we do include them for completeness. Figure 18 shows an example of such comparisons for CH_4, HF, and HNO_3 on 20 August, for O_3, N_2O, CO and HCl on 4 October, and for C_2H_6 on 7 October.

We have calculated the relative differences between the FTIR and smoothed
¹⁰ ACE-FTS partial column amounts of each measured target gas, defined as $100^*(PC_{ACE}-PC_{FTIR})/PC_{FTIR}$, in the altitude range where both FTIR and ACE-FTS are sensitive. These so-called altitude ranges of sensitivity are indicated by the horizontal red lines in Fig. 18. Table 6 lists all comparison results, for each species and each coincident occultation. The above defined relative differences are given (in %) on the
¹⁵ relevant partial column, together with the random error (in %) on the partial column difference, from the combined ACE-FTS and FTIR errors. In the next discussion we will not include the comparisons with the ACE-FTS profiles on 26 October, because of their limited reliability.

For ozone, we obtain relative differences between ACE-FTS and ground-based FTIR
²⁰ varying between −13 and +12%, in the middle troposphere up to the stratopause (∼6 to ∼47 km). For methane and nitrous oxide, the relative differences between ACE-FTS and ground-based FTIR are between −7 and 0% and between −7 and +17%, respectively, in the middle troposphere up to about 30 km. For CO and C_2H_6, the upper altitude limit for the comparison is limited to 20 km; the differences between
²⁵ ACE-FTS and ground-based FTIR vary between −17 and +30% for CO, and between −33 and +37% for C_2H_6. The altitude range for comparison of HCl covers the middle troposphere to about the stratopause; observed differences range from −8 to +34%. In all beforementioned comparisons, the variations in the observed differences are larger than what we expect on the basis of the random errors on the relative differences,

EGU

except for C_2H_6 where the error on the relative difference is very large (237 to 293%) because of the large measurement error for the ground-based FTIR retrievals for this species. For HF, we have only one reliable comparison on 20 August, for which the relative difference between the ACE-FTS and the ground-based FTIR partial column in the range 14 to 40 km is about −3%, whereas the random error on this difference is 7%. Comparisons for HNO_3 in the range 17 to 30 km, show differences between −27 and +29%. In the latter case, the random error on the relative difference is extremely large, because of the large measurement error on the ground-based FTIR HNO_3 partial column.

5.4 FTIR versus HALOE

In the same way as we did for ACE-FTS, we have compared our ground-based FTIR data with correlative data from HALOE. In order to be conform with the ACE comparisons in this paper, we have calculated the relative differences between the FTIR and smoothed HALOE partial column amounts as $100^*(PC_{HALOE}-PC_{FTIR})/PC_{FTIR}$, in the altitude range where both FTIR and HALOE are sensitive for the target species. Figure 19 shows an example of comparisons between retrieved FTIR and the original and raw and smoothed HALOE profiles of O_3, CH_4, HCl, and HF on 16 September 2004. The horizontal red lines indicate the altitude ranges of sensitivity. Table 7 gives an overview of all comparisons, for each species and each coincident occultation. The relative differences are given (in %) on the relevant partial column, together with the associated DOFS and random error (in %). It appears in Table 7 that the discrepancies between HALOE and ground-based FTIR partial columns are always larger on 14 September 2004 than on the other days. We have verified the HALOE and ground-based FTIR data for that particular day and up to now, we haven't found any good explanation for the larger discrepancies. We therefore don't take into account that day in the current discussion. For HCl and HF, the HALOE partial columns in the range 15 to 45 km and 15 to 40 km, respectively, are smaller than the corresponding FTIR partial columns, by about 7 to 17%. This agrees to some extent with previous findings by

C. Senten et al.

Title Page

Abstract	Introduction
Conclusions	References
Tables	Figures

◄◄ ►►

◄ ►

Back Close

Full Screen / Esc

Printer-friendly Version
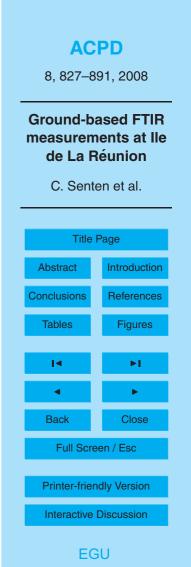
Interactive Discussion

Russell et al. (1996a, 1996b) that HALOE slightly underestimates the HCl and HF vmr profiles. The differences between the HALOE and ground-based FTIR ozone partial columns in the range 10 to 47 km vary between 0 and 15%, with the HALOE profiles being smaller than the ground-based FTIR profiles. For methane, HALOE partial columns in the lower stratosphere (15 to 28 km) are smaller than the ground-based FTIR columns by about 5 to 8%.

6 Conclusion and perspectives

Ground-based FTIR spectroscopy is a very useful technique to derive total column abundances and low-resolution vertical profiles of many important trace gases in the atmosphere. The technique is being used at many stations worldwide, mostly in the frame of NDACC, but rarely at low-altitude tropical or subtropical stations. We have demonstrated the feasibility of performing ground-based FTIR measurements at the (sub)tropical Ile de La Réunion, during two measurement campaigns, in 2002 and 2004. The results presented in this paper show that we can derive total column amounts and some vertical profile information for many of the atmospheric species of interest in tropospheric and stratospheric chemistry. In particular, we have shown that we obtain between 1 and 5 independent pieces of information depending on the species, allowing us to retrieve partial column abundances for O_3, CH_4, N_2O and CO and total column values for HF, HCl, HNO_3 and C_2H_6. Additional species will be investigated in the future.

Total column amounts of CO observed by our ground-based FTIR measurements agree well with correlative space-borne MOPITT observations. The high correlation between the abundances of the gases CO and C_2H_6 confirm that they undergo similar production and destruction processes. More specifically, the total column enhancements in local spring 2004 were due to biomass burning events in southern Africa and Madagascar.

First comparisons showed quite good agreements between the ACE-FTS and

Ground-based FTIR measurements at Ile de La Réunion

C. Senten et al.

EGU

ground-based FTIR profiles of the target gases O_3, N_2O, CH_4, CO, C_2H_6, HNO_3, HF, and HCl, taking into account of course that up to now we only had four satellite over-passes that allow us to check the consistency between both data sets. The same conclusion can be drawn for the comparisons between HALOE and our FTIR profiles of O_3, CH_4, HCl and HF.

It is planned to continue this type of measurements, first on a campaign basis and in the future on a permanent basis. A third campaign is being held in 2007, lasting from May until December; the data will be used for the validation of IASI onboard METOP-1. From 2010 onward, we will be able to make use of a permanent infrastructure at the Maïdo, providing the atmospheric community with continuous ground-based FTIR measurements from this complementary NDACC site. The measurements will con-tribute to the NDACC database and further support satellite validation. As the dataset grows, it will enable contributions to studies of atmospheric processes in the southern subtropics.

References

Anderson, G. P., Chetwynd, J. H., Clough S. A., Kneizys, F. X., and Shettle, E. P.: AFGL atmospheric constituent profiles (0–120 km), Env. Res. Papers, AFGL-TR-86-0110, 1986.

Baray, J. L., Leveau, J., Baldy, S., Jouzel, J., Keckhut, P., Bergametti, G., Ancellet, G., Bencherif, H., Cadet, B., Carleer, M., David, C., De Mazière, M., Faduilhe, D., Beekmann, S. G., Goloub, P., Goutail, F., Metzger, J. M., Morel, B., Pommereau, J. P., Porteneuve, J., Portafaix, T., Posny, F., Robert, L., and Van Roozendael, M.: An instrumented station for the survey of

ozone and climate change in the southern tropics: Scientific motivation, technical description and future plans, J. Environ. Monitor., 8(10), 1020-8, doi:10.1039/b607762e, 2006.

Barret, B., De Mazière, M., and Demoulin, P.: Retrieval and characterisation of ozone profiles from solar infrared spectra at the Jungfraujoch, J. Geophys. Res., 107(D24), 4788, doi:10.1029/2001JD001298, 2002.

Barret, B., De Mazière, M., and Mahieu, E.: Ground-based FTIR measurements of CO from the Jungfraujoch: characterisation and comparison with in-situ surface and MOPITT data, Atmos. Chem. Phys., 3, 2217–2223, 2003,
http://www.atmos-chem-phys.net/3/2217/2003/.

Bernath, P. F., McElroy, C. T., Abrams, M. C., et al.: Atmospheric Chemistry Experiment (ACE): Mission overview, Geophys. Res. Lett., 32, L15S01, doi:10.1029/2005GL022386, 2005.

Boone, C. D., Nassar, R., Walker, K. A., Rochon, Y., McLeod, S. D., Rinsland, C. P., and Bernath, P. F.: Retrievals for the atmospheric chemistry experiment Fourier-transform spectrometer, Appl. Optics, 44(33), 7218–7231, 2005.

Brasseur, G., and Solomon, S.: Aeronomy of the Middle Atmosphere: Chemistry and Physics of the Stratosphere and Mesosphere, D. Reidel Publishing Company, 1984.

Brown, L. R., Farmer, C. B., Rinsland, C. P., and Zander, R.: Remote Sensing of the Atmosphere by High Resolution Infrared Absorption Spectroscopy, in: Spectroscopy of the Earth's Atmosphere and Interstellar Medium, edited by: Rao, K. N. and Weber, A., Academic Press, 1992.

Cronn, D. and Robinson, E.: Tropospheric and Lower Stratospheric Vertical Profiles of Ethane and Acetylene, Geophys. Res. Lett., 6(8), 641–644, 1979.

De Mazière, M., Barret, B., Vigouroux, C., Blumenstock, T., Hase, F., Kramer, I., Camy-Peyret, C., Chelin, P., Gardiner, T., Coleman, M., Woods, P., Ellingsen, K., Gauss, M., Isaksen, I., Mahieu, E., Demoulin, P., Duchatelet, P., Mellqvist, J., Strandberg, A., Velazco, V., Schulz, A., Notholt, J., Sussmann, R., Stremme, W., and Rockmann, A.: Ground-based FTIR measurements of O_3- and climate-related gases in the free troposphere and lower stratosphere, Proceedings of the Quadrennial Ozone Symposium QOS 2004 (Kos, Greece, 1–8 June 2004), P211, 2004.

Emmons, L. K., Deeter, M. N., Gille, J. C., Edwards, D. P., Attié, J.-L., Warner, J., Ziskin, D., Francis, G., Khattatov, B., Yudin, V., Lamarque, J.-F., Ho, S. P., Mao, D., Chen, J. S., Drummond, J., Novelli, P., Sachse, G., Coffey, M. T., Hannigan, J. W., Gerbig, C., Kawakami, S., Kondo, Y., Takegawa, N., Schlager, H., Baehr, J., and Ziereis, H.: Validation

EGU

of Measurements of Pollution in the Troposphere (MOPITT) CO retrievals with aircraft in situ profiles, J. Geophys. Res., 109, D03309, doi:10.1029/2003JD004101, 2004.

Flaud, J.-M., Brizzi, G., Carlotti, M., Perrin, A., and Ridolfi, M.: MIPAS database: Validation of HNO_3 line parameters using MIPAS satellite measurements, Atmos. Chem. Phys., 6, 5037–5048, 2006,
http://www.atmos-chem-phys.net/6/5037/2006/.

Giglio, L., Descloitres, J., Justice, C. O., and Kaufman, Y.,J. : An enhanced contextual fire detection algorithm for MODIS, Remote Sens. Environ., 87(2–3), 273–282, 2003.

Hase, F., Blumenstock, T., and Paton-Walsh, C.: Analysis of the instrumental lineshape of high-resolution Fourier transform IR spectrometers with gas cell measurements and new retrieval software, Appl. Optics, 38, 3417-3422, 1999.

Hase, F., Hannigan, J. W., Coffey, M. T., Goldman, A., Höpfner, M., Jones, N. B., Rinsland, C. P., and Wood, S. W.: Intercomparison of retrieval codes used for the analysis of high-resolution ground-based FTIR measurements, J. Quant. Spectrosc. Ra., 87, 25–52, 2004.

Hawat, T., Stephen, T. M., De Mazière, M., and Neefs, E.: Proceedings SPIE, Acquisition, Tracking and Pointing XVII, edited by: Masten, M. K. and Stockum, L. A., Vol. 5082, 13–20, 2003.

Hyer, E. J., Allen, D. J., and Kasischke, E. S.: Examining injection properties of boreal forest fires using surface and satellite measurements of CO transport, J. Geophys. Res., 112, D18307, doi:10.1029/2006JD008232, 2007.

Meier, A., Toon, G. C., Rinsland, C. P., Goldman, A., and Hase, F.: Spectroscopic atlas of atmospheric micro-windows in the middle infrared, 2nd edition, IRF Technical Report 048, IRF Institute for Rymdfysik, Kiruna, 2004.

Neefs, E., De Mazière, M., Scolas, F., Hermans, C., and Hawat, T.: BARCOS, an automation and remote control system for atmospheric observations with a Bruker interferometer, Rev. Sci. Instrum., 78(3), 035109, doi:10.1063/1.2437144, 2007.

Oelhaf, H., Blumenstock, T., De Mazière, M., Mikuteit, S., Vigouroux, C., Wood, S., Bianchini, G., Baumann, R., Blom, C., Cortesi, U., Liu, G. Y., Schlager, H., Camy-Peyret, C., Catoire, V., Pirre, M., Strong, K., and Wetzel, G.: Validation of MIPAS-ENVISAT version 4.61 HNO_3 operational data by stratospheric balloon, aircraft and ground-based measurements, Proceedings of ACVE-2, ESA-ESRIN, Italy, 2004.

Park, J. H., Russel III, J. M., Gordley, L. L., Drayson, S. R., Benner, D. C., McInerney, J. M., Gunson, M. R., Toon, G. C., Sen, B., Blavier, J.-F., Webster, C. R., Zipf, E. C., Erdman, P.,

Title Page

Abstract | Introduction

Conclusions | References

Tables | Figures

◄ | ►►

◄ | ►

Back | Close

Full Screen / Esc

Printer-friendly Version

Interactive Discussion

EGU

Schmidt, U., and Schiller, C.: Validation of Halogen Occultation Experiment CH_4 measurements from the UARS, J. Geophys. Res., 101(D6), 10 183–10 204, 1996.

Perrin, A., Orphal, J., Flaud, J.-M., Klee, S., Mellau, G., Mäder, H., Walbrodt, D., and Winnewisser, M.: New analysis of the v_5 and $2v_9$ bands of HNO_3 by infrared and millimeter wave techniques: line positions and intensities, J. Mol. Spectrosc., 228, 375–391, 2004.

Randriambelo, T., Baray, J. L., and Baldy, S.: Effect of biomass burning, convective venting, and transport on tropospheric ozone over the Indian Ocean: Reunion Island field observations, J. Geophys. Res., 105(D9), 11 813–11 832, 2000.

Reisinger, A. R., Jones, N. B., Matthews, W. A., and Rinsland, C. P.: Southern hemisphere ground based measurements of Carbonyl Fluoride (COF_2) and Hydrogen Fluoride (HF): Partitioning between flouride reservoir species, Geophys. Res. Lett., 21(9), 797–800, 1994.

Rinsland, C. P., Nicholas, B. J., Connor, B. J., Logan, J. A., Pougatchev, N. S., Goldman, A., Murcray, F. J., Stephen, T. M., Pine, A. S., Zander, R., Mahieu, E., and Demoulin, P.: Northern and southern hemisphere ground-based infrared spectroscopic measurements of tropospheric carbon monoxide and ethane, J. Geophys. Res., 103(D21), 28 197–28 218, 1998.

Rinsland, C. P., Mahieu, E., Zander, R., Jones, N. B., Chipperfield, M. P., Goldman, A., Anderson, J., Russel III, J. M., Demoulin, P., Notholt, J., Toon, G. C., Blavier, J.-F., Sen, B., Sussmann, R., Wood, S. W., Meier, A., Griffith, D. W. T., Chiou, L. S., Murcray, F. J., Stephen, T. M., Hase, F., Mikuteit, S., Schultz, A., and Blumenstock, T.: Long-term trends of organic chlorine from ground-based infrared solar spectra: Past increases and evidence for stabilization, J. Geophys. Res., 108(D8), 4252, doi:10.1029/2002JD003001, 2003.

Rodgers, C. D.: Inverse Methods for Atmospheric Sounding: Theory and Practice, Series on Atmospheric, Oceanic and Planetary Physics, Vol. 2, World Scientific, Singapore, 2000.

Rodgers, C. D. and Connor, B. J.: Intercomparison of remote sounding instruments, J. Geophys. Res., 108(D3), 4116, doi:10.1029/2002JD002299, 2003.

Rothman, L. S., Jacquemart, D., Barbe, A., Benner, D. C., Birk, M., Brown, L. R., Carleer, M. R., Chackerian Jr., C., Chance, K., Coudert, L. H., Dana, V., Devi, V. M., Flaud, J. M., Gamache, R. R., Goldman, A., Hartmann, J. M., Jucks, K. W., Maki, A. G., Mandin, J. Y., Massie, S. T., Orphal, J., Perrin, A., Rinsland, C. P., Smith, M. A. H., Tennyson, J., Tolchenov, R. N., Toth, R. A., Vander, J., Varanasi, P., and Wagner, G.: The Hitran 2004 molecular spectroscopic database, J. Quant. Spectrosc. Ra., 96, 139–204, 2005.

Ground-based FTIR measurements at Ile de La Réunion

C. Senten et al.

EGU

Rudolph, J. and Ehhalt, D. H.: Measurements of C2-C5 hydrocarbons over the North Atlantic, J. Geophys. Res., 86(C12), 11 959–11 964, 1981.

Russell III, J. M., Deaver, L. E., Luo, M., Park, J. H., Gordley, L. L., Tuck, A. F., Toon, G. C., Gunson, M. R., Traub, W. A., Johnson, D. G., Jucks, K. W., Murcray, D. G., Zander, R., Nolt, I. G., and Webster, C. R.: Validation of hydrogen chloride measurements made by the Halogen Occultation Experiment from the UARS platform, J. Geophys. Res., 101(D6), 10 151–10 162, 1996a.

Russell III, J. M., Deaver, L. E., Luo, M., Cicerone, R. J., Park, J. H., Gordley, L. L., Toon, G. C., Gunson, M. R., Traub, W. A., Johnson, D. G., Jucks, K. W., Zander, R., and Nolt, I. G.: Validation of hydrogen fluoride measurements made by the Halogen Occultation Experiment from the UARS platform, J. Geophys. Res., 101(D6), 10 163–10 174, 1996b.

Smit, H. G. J. and Straeter, W.: JOSIE-2000, Jülich Ozone Sonde Intercomparison Experiment 2000, The 2000 WMO international intercomparison of operating procedures for ECC-ozone sondes at the environmental simulation facility at Jülich, WMO Global Atmosphere Watch report series, No. 158, World Meteorological Organization, Geneva, 2004.

Smith, M. A. H.: Compilation of atmospheric gas concentration profiles from 0 to 50 km, NASA TM 83289, 1982.

Stohl, A., Hittenberger, M., and Wotawa, G.: Validation of the Lagrangian particle dispersion model FLEXPART against large scale tracer experiment data, Atmos. Environ., 24, 4245–4264, 1998.

Stohl, A., Forster, C., Frank, A., Seibert, P., and Wotawa, G.: Technical Note: The Lagrangian particle dispersion model FLEXPART version 6.2., Atmos. Chem. Phys., 5, 2461–2474, 2005,
http://www.atmos-chem-phys.net/5/2461/2005/.

Urban, J., Lautié, N., Le Flochmoën, E., Jiménez, C., Eriksson, P., de La Noë, J., Dupuy, E., Ekström, M., El Amraoui, L., Frisk, U., Murtagh, D., Olberg, M., and Ricaud, P.: Odin/SMR limb observations of stratospheric trace gases: Level 2 processing of ClO, N_2O, HNO_3, and O_3, J. Geophys. Res., 110, D14307, doi:10.1029/2004JD005741, 2005.

U.S. National Oceanic and Atmospheric Administration: U.S. Standard Atmosphere: 1976 published by the U.S. Government Printing Office, Washington, D.C., 1976.

EGU

Van der Werf, G. R., Randerson, J. T., Giglio, L., Collatz, G. J., and Kasibhatla, P. S.: Interannual variability in global biomass burning emission from 1997 to 2004, Atmos. Chem. Phys., 6, 3423–3441, 2006,
http://www.atmos-chem-phys.net/6/3423/2006/.

Wang, D. Y., Höpfner, M., Blom, C. E., Ward, W. E., Fischer, H., Blumenstock, T., Hase, F., Keim, C., Liu, G. Y., Mikuteit, S., Oelhaf, H., Wetzel, G., Cortesi, U., Mencaraglia, F., Bianchini, G., Redaelli, G., Pirre, M., Catoire, V., Huret, N., Vigouroux, C., De Mazière, M., Mahieu, E., Demoulin, P., Wood, S., Smale, D., Jones, N., Nakajima, H., Sugita, T., Urban, J., Murtagh, D., Boone, C. D., Bernath, P. F., Walker, K. A., Kuttippurath, J., Kleinböhl, A., Toon, G., and Piccolo, C.: Validation of MIPAS HNO_3 operational data, Atmos. Chem. Phys. Discuss., 7, 5173–5251, 2007,
http://www.atmos-chem-phys-discuss.net/7/5173/2007/.

WMO WDCGG Data Summary: WDCGG No. 30, GAW Data, Volume IV Greenhouse Gases and Other Atmospheric Gases, published by Japan Meteorological Agency, in co-Operation with the World Meteorological Organization, March 2006.

Zander, R., Mahieu, E., Demoulin, P., Duchatelet, P., Servais, C., Roland, G., Delbouille, L., De Mazière, M., and Rinsland, C. P.: Evolution of a dozen non-CO_2 greenhouse gases above Central Europe since the mid-1980s, Environmental Sciences, 2(2–3), 295–303, 2005.

Zhao, Y., Strong, K., Kondo, Y., Koike, M., Matsumi, Y., Irie, H., Rinsland, C. P., Jones, N. B., Suzuki, K., Nakajima, H., Nakane, H., and Murata, I.: Spectroscopic measurements of tropospheric CO, C2H6,C2H2, and HCN in northern Japan, J. Geophys. Res., 107(D18), 4343, doi:10.1029/2001JD000748, 2002.

EGU

Table 1. Source information, altitude range of the obtained a priori variability vector and HWHM of the Gaussian off-diagonal elements of $\mathbf{S}_a$ for each molecule.

Molecule	Source	Alt. range [km]	HWHM [km]
O_3	HALOE	10.6–86.8	5
CH_4	HALOE	14.2–78.4	6
N_2O	ACE	7.0–58.8	6
CO	MOPITT	4.6–16.6	5
C_2H_6	ACE	10.6–20.2	3
HCl	HALOE	15.4–58.8	7
HF	HALOE	15.4–64.4	6
HNO_3	Odin	20.2–34.8	4

ACPD

8, 827–891, 2008

Ground-based FTIR measurements at Ile de La Réunion

C. Senten et al.

Title Page

| Abstract | Introduction |

| Conclusions | References |

| Tables | Figures |

|◄ | ►|

◄ | ►

Back | Close

Full Screen / Esc

Printer-friendly Version

Interactive Discussion

EGU

Table 2. Summary of the retrieval characteristics for each target species, for the campaigns at Maïdo, 2002, and St-Denis, 2004. Variab. represents the diagonal elements of $\mathbf{S}_a$ and HWHM the inter-layer correlation length in $\mathbf{S}_a$. The fourth and fifth columns list the spectral micro-windows that are fitted simultaneously and the associated spectral resolution. SNR is the ad-hoc signal-to-noise ratio adopted in the retrievals. The last column provides the achieved mean DOFS.

Molecule	Variab. [%]	HWHM [km]	Micro-window(s) [cm^{-1}]	Spectral resolution [cm^{-1}]	SNR	Interfering species	DOFS Maïdo / St-Denis
O_3	20	6	1000.00–1005.00	0.0072	150	H_2O	4.9/5.1
CH_4	variable	5	2613.70–2615.40	0.00513	250	HDO, H_2O	2.2/2.4
			2650.60–2651.30			(fitted	
			2835.50–2835.80			first), CO_2	
			2903.60–2904.03				
			2921.00–2921.60				
N_2O	10	5	2481.30–2482.60	0.00513	150	CO_2, CH_4,	3.0/3.2
			2526.40–2528.20			O_3, H_2O,	
			2537.85–2538.80			HDO	
			2540.10–2540.70				
CO	20	4	2057.70–2057.91	0.0036	150	O_3, OCS, CO_2,	2.6 / 2.8
			2069.55–2069.72			N_2O, H_2O,	
			2157.40–2159.35			solar CO lines	
C_2H_6	40	5	2976.50–2977.20	0.00513	250	H_2O, CH_4, O_3	1.5/1.7
HCl	20	5	2843.30–2843.80	0.00513	150	H_2O, CH_4, HDO	1.2/1.4
			2925.70–2926.60				
HF	20	3	4038.70–4039.05	0.0072	300	H_2O	1.4/1.5
HNO_3	20	5	872.25–874.80	0.01098	200	OCS, C_2H_6, H_2O	1.0/1.2

Table 3. Summary of the error budgets (in %) on the total (2.2–100 km) and partial columns (altitude ranges specified in km) for each target species retrieved from the Ile de La Réunion campaign data, for Maïdo 2002.
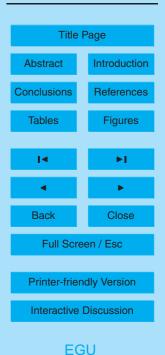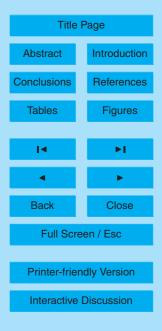
Molecule	Temp. error [%]	FM param. error [%]	Meas. error [%]	Smooth. Error [%]	Total random error [%]	Line intens. [%]	Air broad. [%]	Total syst. error [%]
O_3								
2.2–100	0.45	0.04	0.30	0.92	1.07	4.60	0.48	4.63
2.2–8.2	0.10	0.29	3.90	16.38	16.84	4.77	5.94	7.62
8.2–17.8	1.40	0.65	5.24	14.25	15.26	7.01	6.95	9.87
17.8–23.8	1.12	0.29	3.01	6.28	7.06	5.43	7.88	9.57
23.8–31.0	1.89	0.21	2.57	2.68	4.17	5.22	2.28	5.70
31.0–100	1.92	0.10	1.96	2.49	3.70	4.83	4.03	6.29
CH_4								
2.2–100	0.95	0.07	0.33	0.18	1.03	19.65	3.13	19.90
2.2–13.0	0.57	0.11	0.56	0.23	0.83	20.23	0.93	20.25
13.0–100	2.44	0.72	1.16	0.93	2.95	17.46	16.92	24.31
N_2O								
2.2–100	0.12	0.11	0.09	0.18	0.27	4.67	0.85	4.74
2.2–4.6	1.00	0.24	0.69	1.49	1.94	4.48	8.88	9.94
4.6–15.4	0.11	0.08	0.32	0.82	0.90	4.74	4.17	6.31
15.4–100	0.80	1.06	0.75	0.72	1.69	4.91	5.61	7.45

Table 3. Continued.

Molecule	Temp. error [%]	FM param. error [%]	Meas. error [%]	Smooth. Error [%]	Total random error [%]	Line intens. [%]	Air broad. [%]	Total syst. error [%]
CO								
2.2–100	0.90	0.14	2.44	0.22	2.61	4.59	0.33	4.60
2.2–13.0	1.04	0.15	3.00	0.73	3.26	4.68	0.77	4.75
13.0–100	0.47	0.21	20.48	5.76	21.29	3.88	4.21	5.73
C_2H_6								
2.2–100	0.52	0.20	33.98	1.43	34.01	16.93	6.14	18.01
HCl								
2.2–100	0.31	1.38	4.47	17.79	18.39	2.87	11.64	11.99
HF								
2.2–100	0.22	0.24	8.87	7.71	11.76	17.90	0.98	17.93
HNO_3								
2.2–100	0.77	0.60	34.08	26.41	43.12	15.43	2.33	15.60

EGU

Table 4. Summary of the error budgets (in %) on the total (0.05–100 km) and partial columns (altitude ranges specified in km) for each target species retrieved from the Ile de La Réunion campaign data, for St-Denis 2004.

Molecule	Temp. error [%]	FM param. error [%]	Meas. error [%]	Smooth. Error [%]	Total random error [%]	Line intens. [%]	Air broad. [%]	Total syst. error [%]
O$_3$								
0.05–100	0.50	0.02	0.28	0.30	0.65	4.73	0.39	4.75
0.05–8.2	0.08	0.07	3.02	6.18	6.88	4.79	3.86	6.16
8.2–17.8	1.91	0.10	4.41	10.49	11.54	5.18	4.81	7.07
17.8–23.8	1.46	0.04	2.79	6.36	7.10	4.76	6.85	8.34
23.8-31.0	2.68	0.12	2.71	6.16	7.24	4.87	1.96	5.25
31.0–100	1.84	0.10	2.10	5.40	6.08	5.06	3.81	6.34
CH$_4$								
0.05–100	1.07	0.04	0.50	0.19	1.20	19.81	3.15	20.06
0.05-4.6	0.73	0.12	0.76	0.24	1.09	20.30	0.55	20.31
15.4–100	2.76	0.75	1.63	1.34	3.55	17.45	16.74	24.18
N$_2$O								
0.05–100	0.18	0.12	0.07	0.12	0.26	4.60	0.79	4.67
0.05–4.6	0.80	0.16	0.29	0.86	1.22	4.68	6.94	8.37
4.6–15.4	0.34	0.12	0.25	1.16	1.24	4.61	7.15	8.51
15.4–100	0.20	1.55	0.72	1.10	2.04	4.36	4.82	6.50

Ground-based FTIR measurements at Ile de La Réunion

C. Senten et al.

[EGU](#)

Table 4. Continued.

Molecule	Temp. error [%]	FM param. error [%]	Meas. error [%]	Smooth. Error [%]	Total random error [%]	Line intens. [%]	Air broad. [%]	Total syst. error [%]
CO								
0.05–100	1.06	0.22	0.57	0.50	1.32	4.69	0.24	4.69
0.05–13.0	1.05	0.24	0.63	1.18	1.72	4.73	0.56	4.76
13.0–100	1.26	0.23	2.96	7.71	8.36	4.27	3.09	5.27
C_2H_6								
0.05–100	0.99	0.63	75.68	1.69	75.70	18.73	3.88	19.13
HCl								
0.05–100	0.16	0.22	8.62	10.74	13.77	3.00	7.52	8.10
HF								
0.05–100	0.14	0.14	9.48	13.76	16.72	3.38	0.19	3.38
HNO_3								
0.05–100	1.26	0.74	90.10	24.13	93.28	29.45	6.96	30.26

EGU

Table 5. Relative differences (in %) between O_3 partial columns from sonde and FTIR measurements at Ile de La Réunion on 4 days of coincident observations. DOFS gives the number of degrees of freedom for the partial column in the considered altitude range, which is the sensitivity range of both instruments. The last column provides the percentage random error associated with the relative difference, from the combined sonde and FTIR errors.

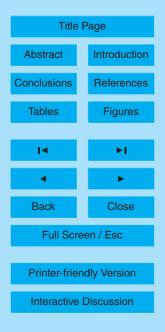| Date	Altitude range [km]	DOFS	Rel. diff. [%]	Error [%]
18 August 2004	0.05–28.6	3.67	0.47	2.00
1 September 2004	0.05–32.2	4.11	4.74	1.94
16 September 2004	0.05–31.0	3.78	8.08	1.92
4 October 2004	0.05–33.4	4.46	4.42	1.93

Table 6. Relative differences (in %) between ACE-FTS and high sensitivity FTIR partial columns at Ile de La Réunion in 2004 for each common measured species, together with the combined error (in %) on that partial column.

Molecule	Date	Altitude range [km]	DOFS	Rel. diff. [%]	Error [%]
O_3	20 August 2004	5.8–47.4	4.18	−3.74	0.88
	3 October 2004	5.8–47.4	4.33	11.79	0.79
	4 October 2004	8.2–47.4	4.08	6.56	0.76
	6 October 2004	5.8–36.4	3.46	−12.50	1.14
	26 October 2004	16.6–47.4	3.19	−2.78	0.89
CH_4	20 August 2004	7.0–28.6	1.35	−5.93	1.33
	3 October 2004	5.8–28.6	1.42	−4.97	1.18
	4 October 2004	8.2–28.6	1.20	−6.34	1.79
	6 October 2004	5.8–28.6	1.60	−0.217	1.10
	26 October 2004	16.6–28.6	0.56	2.09	2.74
N_2O	20 August 2004	5.8–25.0	1.75	−6.97	0.61
	3 October 2004	5.8–31.0	2.02	−3.06	0.73
	4 October 2004	8.2–31.0	1.70	−4.36	0.73
	6 October 2004	5.8–28.6	6.57	16.51	0.70
	26 October 2004	16.6–25.0	0.70	13.04	2.25
CO	20 August 2004	7.0–19.0	1.19	−16.49	2.36
	3 October 2004	5.8–19.0	1.31	29.74	2.93
	4 October 2004	8.2–19.0	0.96	−16.74	2.87
	26 October 2004	16.6–20.2	0.10	−3.07	3.28

Table 6. Continued.

Molecule	Date	Altitude range [km]	DOFS	Rel. diff. [%]	Error [%]
C_2H_6	20 August 2004	8.2–20.2	0.88	−12.30	292.69
	3 October 2004	7.0–20.2	1.24	36.60	241.17
	4 October 2004	8.2–20.2	1.16	−31.41	292.70
	6 October 2004	7.0–19.0	0.78	−32.59	237.32
	26 October 2004	17.8–20.2	0.09	−43.08	1140.67
HCl	20 August 2004	8.2–47.4	1.38	9.93	10.29
	3 October 2004	9.4–42.4	1.28	33.71	10.51
	4 October 2004	9.4–42.4	1.28	15.36	10.51
	6 October 2004	8.2–47.4	1.25	−7.50	10.36
	26 October 2004	16.6–44.8	1.07	−20.07	9.98
HF	20 August 2004	14.2–40.2	1.14	−3.38	7.44
	26 October 2004	17.8–38.2	1.07	−38.04	7.92
HNO_3	20 August 2004	16.6–32.2	0.93	3.36	137.58
	3 October 2004	16.6–28.6	1.09	29.18	150.92
	4 October 2004	16.6–28.6	1.09	5.56	150.92
	6 October 2004	16.6–32.2	1.03	−26.51	137.58
	26 October 2004	16.6–28.6	0.97	−38.44	150.92

Table 7. Relative differences (in %) between HALOE and high sensitivity FTIR partial columns at Ile de La Réunion in 2004 for each common measured species, together with the combined error (in %) on that partial column.

Molecule	Date	Sens. range [km]	DOFS	Rel. diff. [%]	Error [%]
O_3	29 August 2004	10.6–47.4	3.66	−0.71	0.90
	30 August 2004	10.6–47.4	3.54	−8.64	0.81
	31 August 2004	10.6–50.8	3.61	−13.80	0.87
	14 September 2004	10.6–42.4	3.32	−44.06	17.71
	15 September 2004	10.6–50.8	3.63	−12.29	0.89
	16 September 2004	10.6–47.4	3.46	−15.08	0.87
CH_4	29 August 2004	14.2–28.6	0.71	−7.16	3.32
	30 August 2004	14.2–28.6	0.70	−8.13	3.32
	31 August 2004	14.2–28.6	0.70	−5.09	3.32
	14 September 2004	14.2–28.6	0.69	−4.65	3.32
	15 September 2004	14.2–28.6	0.69	−5.42	3.32
	16 September 2004	14.2–28.6	0.72	−4.56	3.33
HCl	29 August 2004	15.4–44.8	1.09	12.53	16.77
	30 August 2004	15.4–44.8	1.00	−7.56	13.38
	31 August 2004	15.4–23.8	1.91	−14.16	32.16
	14 September 2004	15.4–44.8	1.20	−38.11	10.25
	15 September 2004	16.6–47.4	0.74	−14.40	9.73
	16 September 2004	15.4–44.8	1.51	2.06	10.24
HF	29 August 2004	15.4–40.2	1.15	9.32	10.78
	30 August 2004	15.4–40.2	1.18	−7.65	7.53
	31 August 2004	15.4–40.2	1.17	−12.21	7.95
	14 September 2004	15.4–40.2	1.13	−36.31	8.61
	15 September 2004	15.4–38.2	1.11	−17.04	7.67
	16 September 2004	15.4–38.2	1.10	−0.37	7.67

EGU

EGU

Fig. 1. Composite spectra for different bandpass filters (NDSC-1: red, NDSC-2: blue, NDSC-3: dark blue, NDSC-5: green, and NDSC-6: pink), taken at Maïdo (upper plot) and at St-Denis (bottom plot) in 2002, for solar zenith angles between 40˚ and 50˚.

Fig. 2. A priori uncertainties (in %) in the volume mixing ratios as a function of the altitude, for each retrieved trace gas at Ile de La Réunion.

Fig. 3. Temperature covariance matrix (in K^2) from NCEP and ECMWF temperature profiles at Ile de La Réunion in October 2004.

Fig. 4. Time series of the total column amounts (in molecules/cm^2) at St-Denis in 2002 and 2004 for all retrieved species.
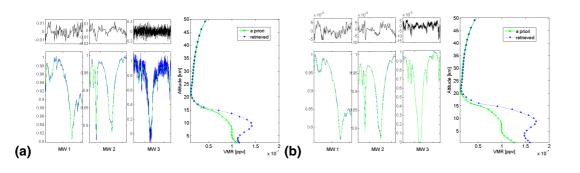
Fig. 5. Single micro-window fit of O_3 plus interfering species from a single spectrum on **(a)** 13 October 2002 at Maïdo and on **(b)** 15 October 2004 at St-Denis. Measured (blue) and simulated spectra (green) are shown (left lower plot), together with the residuals (left upper plot), computed as measured minus simulated, and the a priori (green crosses) and retrieved profile (blue diamonds) (right plot).
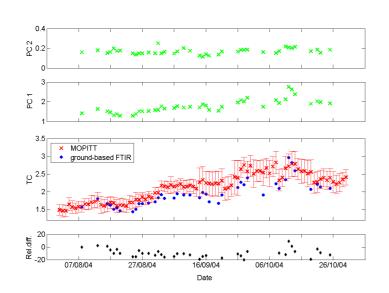
EGU

Fig. 6. Multiple micro-window fit of CH_4 plus interfering species from a single spectrum on **(a)** 16 October 2002 at Maïdo and on **(b)** 12 October 2004 at St-Denis. Measured (blue) and simulated spectra (green) are shown (left lower plot), together with the residuals (left upper plot), computed as measured minus simulated, and the a priori (green crosses) and retrieved profile (blue diamonds) (right plot).
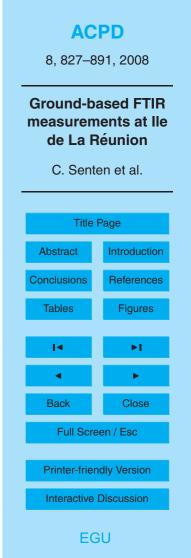
Fig. 7. Multiple micro-window fit of N_2O plus interfering species from a single spectrum on **(a)** 16 October 2002 at Maïdo and on **(b)** 12 October 2004 at St-Denis. Measured (blue) and simulated spectra (green) are shown (left lower plot), together with the residuals (left upper plot), computed as measured minus simulated, and the a priori (green crosses) and retrieved profile (blue diamonds) (right plot).

EGU

Fig. 8. Multiple micro-window fit of CO plus interfering species from a single spectrum on **(a)** 19 October 2002 at Maïdo and on **(b)** 12 October 2004 at St-Denis. Measured (blue) and simulated spectra (green) are shown (left lower plot), together with the residuals (left upper plot), computed as measured minus simulated, and the a priori (green crosses) and retrieved profile (blue diamonds) (right plot).

EGU

Fig. 9. From top to bottom: Time series from the period August–October 2004 of daily mean CO abundances (in 10^{18} molecules/cm^2) measured by the ground-based FTIR instrument at St-Denis, in the 13–100 km layer (PC2), in the surface to 13 km layer (PC1), and in 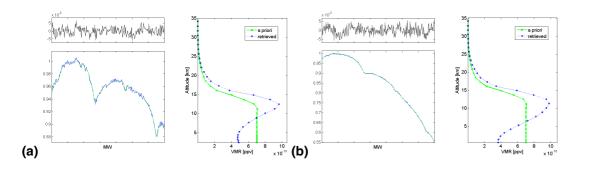the total column (TC, blue circles). The latter plot includes the daily mean CO total column amounts and associated standard deviations measured by MOPITT (red crosses). The lowest plot shows the percentage relative differences between the MOPITT and ground-based FTIR data for the CO total columns, on coincident days.

Fig. 10. Time series of CO abundances at St-Denis between 0 and 13 km, in October 2004, calculated by ground-based FTIR (blue diamonds) and FLEXPART with (1) GFED emissions (pink squares), (2) GFED emissions ×2 (yellow triangles), (3) GFED emissions ×4 (green triangles).

ACPD

8, 827–891, 2008

Ground-based FTIR measurements at Ile de La Réunion

C. Senten et al.

Title Page

Abstract   Introduction

Conclusions   References

Tables   Figures

◄◄   ►►

◄   ►

Back   Close

Full Screen / Esc

Printer-friendly Version

Interactive Discussion

EGU

Fig. 11. Total amount of CO emitted and transported (in kg) to Ile de La Réunion (located within the red circle) on 12 October 2004, calculated by FLEXPART.

(a) **(b)**

Fig. 12. Single micro-window fit of C_2H_6 plus interfering species from a single spectrum on **(a)** 14 October 2002 at Maïdo and on **(b)** 9 October 2004 at St-Denis. Measured (blue) and simulated spectra (green) are shown (left lower plot), together with the residuals (left upper plot), computed as measured minus simulated, and the a priori (green crosses) and retrieved profile (blue diamonds) (right plot).
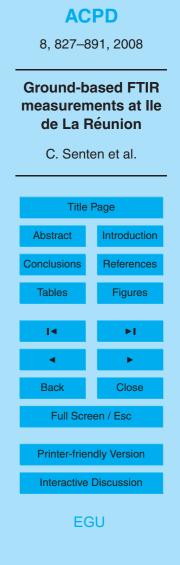
Fig. 13. Correlation plot of CO versus C_2H_6 total column amounts (in molecules/cm^2) during the FTIR campaigns at St-Denis in 2002 and 2004.
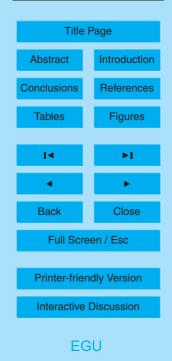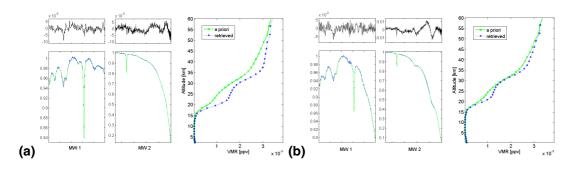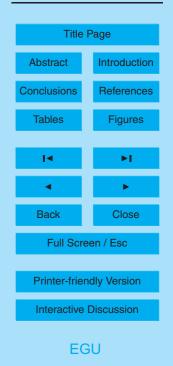
(a) **(b)**

Fig. 14. Multiple micro-window fit of HCl plus interfering species from a single spectrum on **(a)** 16 October 2002 at Maïdo and on **(b)** 15 October 2004 at St-Denis. Measured (blue) and simulated spectra (green) are shown (left lower plot), together with the residuals (left upper plot), computed as measured minus simulated, and the a priori (green crosses) and retrieved profile (blue diamonds) (right plot).

EGU

ACPD

8, 827–891, 2008

Ground-based FTIR measurements at Ile de La Réunion

C. Senten et al.

Title Page

Abstract | Introduction

Conclusions | References

Tables | Figures

◀◀ | ▶▶

◀ | ▶

Back | Close

Full Screen / Esc

Printer-friendly Version

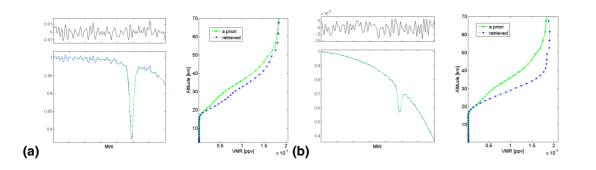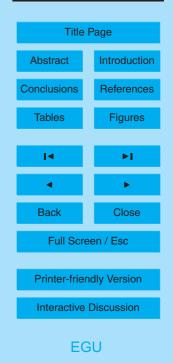Interactive Discussion

EGU

(a)   **(b)**

Fig. 15. Single micro-window fit of HF plus interfering species from a single spectrum on **(a)** 13 October 2002 at Maïdo and on **(b)** 11 October 2004 at St-Denis. Measured (blue) and simulated spectra (green) are shown (left lower plot), together with the residuals (left upper plot), computed as measured minus simulated, and the a priori (green crosses) and retrieved profile (blue diamonds) (right plot).
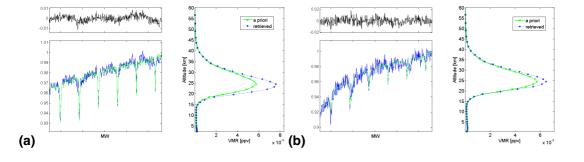
(a) (b)

Fig. 16. Single micro-window fit of HNO$_3$ plus interfering species from a single spectrum on **(a)** 16 October 2002 at Maïdo and on **(b)** 21 October 2004 at St-Denis. Measured (blue) and simulated spectra (green) are shown (left lower plot), together with the residuals (left upper plot), computed as measured minus simulated, and the a priori (green crosses) and retrieved profile (blue diamonds) (right plot).
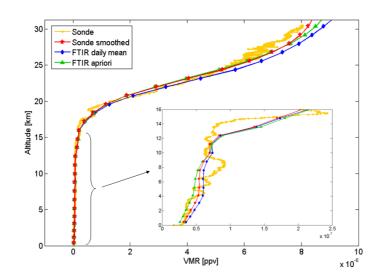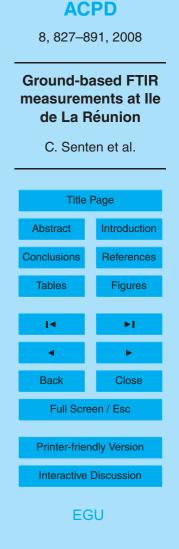
Fig. 17. Comparison of O_3 vertical profiles at St-Denis on 16 September 2004 obtained from ground-based FTIR (blue diamonds) and O_3 sonde (yellow dots). Green triangles indicate the a priori FTIR profile and red stars the sonde profile smoothed by the FTIR averaging kernels.
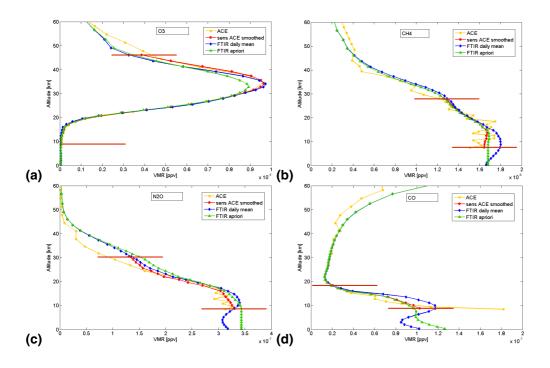
EGU

Fig. 18. Vertical vmr profiles from 0 to 60 km of **(a)** O_3 on 4 October, **(b)** CH_4 on 20 August, **(c)** N_2O on 4 October, **(d)** CO on 4 October, **(e)** C_2H_6 on 7 October, **(f)** HCl on 4 October, **(g)** HF on 20 August, and **(h)** HNO_3 on 20 August, measured at St-Denis in 2004 by ground-based FTIR (blue diamonds) and by ACE-FTS (raw: yellow circles; smoothed: red stars). The FTIR a priori profile is indicated by the green triangles.
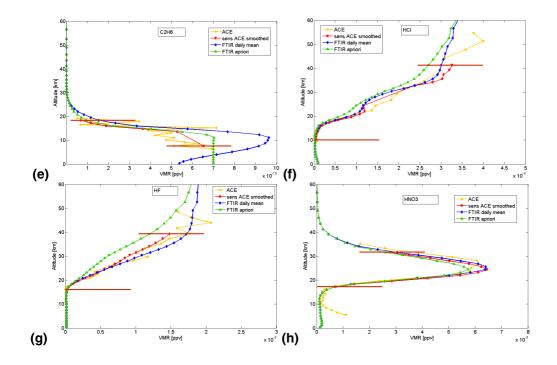
Title Page

Abstract | Introduction

Conclusions | References

Tables | Figures

|◄ | ►|

◄ | ►

Back | Close

Full Screen / Esc

Printer-friendly Version

Interactive Discussion

EGU

Fig. 18. Continued.

Fig. 19. Vertical vmr profiles form 0 to 60 km of **(a)** O$_3$, **(b)** CH$_4$, **(c)** HCl and **(d)** HF, measured at St-Denis by ground-based FTIR (blue diamonds) and by HALOE (raw: yellow circles; smoothed: red stars) on 16 September 2004. The green triangles indicate the a priori FTIR profile.

Title Page

Abstract   Introduction

Conclusions   References

Tables   Figures

◀◀   ▶▶

◀   ▶

Back   Close

Full Screen / Esc

Printer-friendly Version

Interactive Discussion